PCCP

Cite this: *Phys. Chem. Chem. Phys.*, 2011, **13**, 20262–20274

www.rsc.org/pccp

PAPER

High-temperature oxidation chemistry of *n*-butanol – experiments in low-pressure premixed flames and detailed kinetic modeling†

N. Hansen,*[a] M. R. Harper[b] and W. H. Green*[b]

Received 24th May 2011, Accepted 15th September 2011
DOI: 10.1039/c1cp21663e

An automated reaction mechanism generator is used to develop a predictive, comprehensive reaction mechanism for the high-temperature oxidation chemistry of *n*-butanol. This new kinetic model is an advancement of an earlier model, which had been extensively tested against earlier experimental data (Harper *et al.*, *Combust. Flame*, 2011, **158**, 16–41). In this study, the model's predictive capabilities are improved by targeting isomer-resolved quantitative mole fraction profiles of flame species in low-pressure flames. To this end, a total of three burner-stabilized premixed flames are isomer-selectively analyzed by flame-sampling molecular-beam time-of-flight mass spectrometry using photoionization by tunable vacuum-ultraviolet synchrotron radiation. For most species, the newly developed chemical kinetic model is capable of accurately reproducing the experimental trends in these flames. The results clearly indicate that *n*-butanol is mainly consumed by H-atom abstraction with H, O, and OH, forming predominantly the α-C_4H_9O radical ($CH_3CH_2CH_2{}^{\bullet}CHOH$). Fission of C–C bonds in *n*-butanol is only predicted to be significant in a similar, but hotter flame studied by Oßwald *et al.* (*Combust. Flame*, 2011, **158**, 2–15). The water-elimination reaction to 1-butene is found to be of no importance under the premixed conditions studied here. The initially formed isomeric C_4H_9O radicals are predicted to further oxidize by reacting with H and O_2 or to decompose to smaller fragments *via* β-scission. Enols are detected experimentally, with their importance being overpredicted by the model.

1. Introduction

Concerns over future supply shortages and environmental degradation, *i.e.* climate change and air pollution, have motivated many nations to transition away from conventional, petroleum-based fuel sources and to utilize fuels derived from biomass instead. In particular, there has been a large interest in *n*-butanol (*n*-C_4H_9OH) as an attractive alternative and additive to gasoline.[1,2] As the technology to convert biomass into butanol becomes more sophisticated,[3] the use of butanol as a fuel will quickly gain momentum. This potential impact of butanol on the biofuel sector has evoked particular interest in the combustion community and the importance of accurately characterizing the combustion chemistry of butanol is readily acknowledged. Therefore, several studies have been targeted on a fundamental understanding of its combustion chemistry.[4–23] These previous butanol studies include experiments in and/or detailed modeling of flames,[4–11] static,[12] flow[13,14] and jet-stirred reactors,[7,15–17] shock tubes,[18–22] and a rapid compression machine.[23] However, to review the results of these earlier studies is beyond the scope of the present paper. Most relevant to the current work are the experimental measurements of Yang *et al.*[6] and Oßwald *et al.*[11] in low-pressure premixed flames and the modeling work of Van Geem *et al.*[13] and Harper *et al.*[14]

In the present work, we use the isomer-resolved species mole fraction profiles in the burner-stabilized premixed flames of *n*-butanol to test the predictive capabilities of the comprehensive reaction mechanism currently under development in Green's group.[13,14] This study focuses on advancements in detailed modeling of the combustion chemistry of *n*-butanol and on developments of mechanistic insights into its high-temperature oxidation chemistry in premixed flames. To this end, we use a chemical kinetic model,[13] which has been improved since publication in 2010, and isomer-resolved chemical structures of different premixed low-pressure flames fueled by *n*-butanol to unravel the important chemical pathways of fuel oxidation.

The current chemical kinetic mechanism, which has also been tested against the earlier experimental data (jet-stirred reactors, opposed-flow diffusion flames, rapid compression machines, and shock tubes), is capable of accurately reproducing most experimental trends in the burner-stabilized premixed flames studied here. These flames are: (1) a H_2/O_2-base flame doped with *n*-butanol, (2) a highly diluted flame containing

[a] *Combustion Research Facility, Sandia National Laboratories, Livermore, CA 94551. E-mail: nhansen@sandia.gov*
[b] *Department of Chemical Engineering, Massachusetts Institute of Technology, Cambridge, MA 02139. E-mail: whgreen@mit.edu*
† Electronic supplementary information (ESI) available. See DOI: 10.1039/c1cp21663e

80% Ar, and (3) a *n*-butanol/O_2/Ar flame under stoichiometric conditions. The flame conditions, which are chosen to be neither as fuel-rich nor as concentrated in fuel as the conditions from Yang *et al.*[6] and Oßwald *et al.*,[11] are well suited for this study because molecular-weight growth chemistry is largely inhibited. Therefore, the three new flames reported here are expected to be modeled more easily. Nevertheless, the current model's performance is also evaluated against the recently published experimental low-pressure flame data from Oßwald *et al.*[11]

This study highlights the significant isomer-specific aspects of the flame structures, describes the critical features of the improved *n*-butanol combustion chemistry model, and identifies the important fuel consumption and oxidation sequences.

2. Combustion chemistry modeling

Chemical kinetic reaction mechanisms are often developed in a hierarchical manner, that is, beginning with small molecules (C_0–C_2) and few reactions; larger mechanisms for larger molecules are then constructed by adding more reactions and species, by hand, on top of the mechanisms for the smaller species.[24] However, with the average number of species and reactions steadily increasing in a typical-size mechanism,[25] it becomes less practical to construct models that way. Specifically, it is difficult to guarantee that all cross-reactions between the smaller species and those larger molecules being appended to the base mechanism are considered for inclusion in the full mechanism. In a different approach, the chemical kinetic model employed in this study is constructed using the automated "Reaction Mechanism Generator" (RMG) software package.[26] RMG is a rate-based, automated reaction network generator that constructs pressure-dependent networks for isothermal, isobaric batch systems.

The RMG software can construct reaction mechanisms in a hierarchical manner, utilizing "Seed Mechanisms." Within the RMG package, a "Seed Mechanism" is defined as a user-supplied list of species, reactions, and rate coefficients that must be included in the initial reaction mechanism. The RMG software then proposes new reactions, using the list of species supplied in the Seed Mechanism (*e.g.* the GRI-Mech 3.0 mechanism) and the new larger molecules of interest (*e.g.* *n*-butanol), by comparing each combinatorial possibility against the ~35 reaction family templates in the RMG database. For example, these templates include H-abstraction, β-scission, and recombination reactions. A complete list of reaction family templates can be found elsewhere.[26] Any reactions composed exclusively of those species in the Seed Mechanism are added to the model immediately (the "cross-reactions"); all others are added to the list of non-significant reactions. Applying the rate-based algorithm[27] for the temperature, pressure, and species' concentrations of interest, until the user-specified tolerance is satisfied, results in the final chemical kinetic model.

For this study, the RMG targets are chosen to be the isomer-resolved chemical compositions of the following burner-stabilized flat flames:

Flame 1: *n*-butanol, 24.1% H_2, 24.1% O_2, 48.2% Ar with a fuel/oxygen equivalence ratio $\phi = 1.4$ at a reduced pressure of $p = 15$ Torr and a cold-flow reagent velocity of $v = 132.8$ cm/s;

Flame 2: *n*-butanol, 16.7% O_2, 80.0% Ar, $\phi = 1.2$, $p = 25$ Torr and $v = 76.9$ cm/s;

Flame 3: *n*-butanol, 42.8% O_2, 50.0% Ar, $\phi = 1.0$, $p = 15$ Torr and $v = 96.1$ cm/s.

In addition, the model's predictions are also compared with earlier experimental results of a fuel-rich flame from Oßwald *et al.*:[11]

Flame Oßwald: *n*-butanol, 58.1% O_2, 25% Ar, $\phi = 1.7$, $p = 30$ Torr and $v = 32.3$ cm/s

Using the RMG software package, a reaction mechanism for *n*-butanol oxidation is constructed to match the experimental conditions of Flames 1 and 2. Beginning with the mechanism of ref. 13, each of the 1293 pressure-dependent rate coefficients is re-calculated using the steady-state master equation technique of Green and Bhatti.[28] These calculations are re-done due to incompatible units between different modules in the RMG v3.2 software, causing some of the chemically-activated reactions' rate coefficients to be underestimated by a factor of 10^6; see ref. 29 for more details. Two important findings in that study were: (a) the model's results were not very sensitive to these under-predicted kinetics for the reactor conditions studied, and (b) some of the updated mechanism's kinetics were very fast, leading to stiff matrices when solving the reactor models' ordinary differential equations.

The mechanism from ref. 29 is run through a sub-module of the RMG software (the CheckForwardAndReverseRateCoefficients class) to identify all RMG-generated reaction rate coefficients (either high-p or pressure-dependent) which exceeded 10^{15} s^{-1} or 10^{15} cm^3 mol^{-1} s^{-1} from 300–3000 K, at pressures spanning 15 Torr–100 bar. The majority of these too-fast kinetics is pressure-dependent, and the source of the error is usually an inaccurate radical species thermochemistry, previously estimated using Benson's group additivity and Bozzelli's hydrogen–atom bond increments. The thermochemistry for the 15 offending species is now estimated using quantum chemistry. The enthalpy of formation at 298 K, the entropy at 298 K, and the heat capacity at 300, 400, 500, 600, 800, 1000, and 1500 K are computed for these 15 species, using the standard statistical thermodynamics formulas. The optimized geometry, moment of inertia, and vibrational frequencies are computed in Gaussian 03,[30] using the composite CBS-QB3 method. In calculating the vibrational partition function, low-frequency torsional modes are treated as 1-d separable hindered rotors; the remaining frequencies are treated with the rigid-rotor harmonic oscillator model. Further details are provided elsewhere.[13,14]

To resolve the too-fast kinetics, any pressure-dependent network containing at least one of the 15 species is re-calculated, utilizing the new thermochemistry calculations; all RMG-generated reaction rate coefficients are now less than the 10^{15} threshold discussed previously. Furthermore, the pressure-dependent kinetics on the C_3H_5 potential energy surface calculated by Miller *et al.*[31] replaced the RMG estimated pressure-dependent kinetics. Additionally, the kinetics for all reactions of the form R–$^{\bullet}$CH–OH + O_2 ⇄ HO_2 + R–CH=O are now estimated using the calculation of Zádor *et al.* for $CH_3{}^{\bullet}CHOH + O_2 \rightleftarrows HO_2 + CH_3CHO$.[32] Lastly, the H-abstraction rate coefficients of *n*-butanol by atomic oxygen and hydroxyl radical are revised. The mechanism now estimates the abstraction from *n*-butanol by hydroxyl using the G3 calculations of Zhou *et al.*[33] To the best of our knowledge,

there are no published calculations for abstraction from *n*-butanol by atomic oxygen. Thus, for abstraction from the δ-, α-, and hydroxyl positions of *n*-butanol by atomic oxygen, the rate coefficients are now estimated using the calculations of Wu *et al.*[34] for abstraction from the β-, α-, and hydroxyl positions of ethanol, respectively. For abstraction from the γ- and β-positions of *n*-butanol by atomic oxygen, Cohen and Westberg's experimental branching ratio for abstraction from the secondary carbons of *n*-butane by atomic oxygen to abstraction from the primary carbons of *n*-butane by atomic oxygen[35] is employed. The abstraction from the primary carbons of *n*-butane by atomic oxygen is assumed to be twice the abstraction from the primary carbon of ethanol by atomic oxygen, as estimated by Wu *et al.*; multiplying this rate coefficient by the branching ratio yields our estimate for abstraction from both the γ- and β-positions of *n*-butanol by atomic oxygen.

This updated mechanism is then supplied as a "Seed Mechanism" for the new RMG simulations, to match the experimental conditions of Flames 1 and 2, for this study. The earlier versions[13,14,29] have already been tested against pyrolysis experiments, autoignition delay times, and mole fraction profiles in a jet-stirred reactor, in an opposed-flow diffusion flame, and in a doped methane diffusion flame. Compared to the previous experiments used for model development and testing, the chosen flame conditions here are at a much lower pressure. Thus, many radical-radical reactions that were estimated by RMG not to be significant in the previous studies are now predicted by RMG to be significant and are therefore included in the new reaction mechanism. Every high-*p* limit rate coefficient is corrected for fall-off effects, and the $k(T,p)$ for all chemically-activated reactions within each pressure-dependent network is estimated, using the steady-state master equation technique of Green and Bhatti.[28] The critical features of the newly constructed reaction set will be discussed in section 4 combined with the flame chemistry insights.

The full model is available online as supplemental information.† All model calculations are performed in CHEMKIN-MFC,[36] using the Premix Burner reactor model. The experimentally-measured temperature profile (discussed in Section 3) is supplied as input. The thermal diffusion (Soret) effect is included and the mixture-averaged transport formalism is assumed. The initial grid is uniformly-spaced using 100 grid points. The maximum number of grid points is set to 1000 and the adaptive grid control based on solution gradient and curvature is set to 0.2, which has been found to be an appropriate compromise between accuracy and CPU time. The model's predictions are subsequently compared with experimentally derived mole fraction data from the low-pressure premixed flames. The exact experimental procedures are described next.

3. Experimental procedures

The flames are stabilized at a low pressure on a water-cooled 6-cm diameter stainless steel McKenna burner. The gas flows are controlled by calibrated mass flow controllers, and the liquid fuel is metered by a syringe pump, evaporated, and added into the oxidizer stream. The gases are purchased from Matheson Tri-Gas and *n*-butanol is used as purchased from Sigma-Aldrich. Their quoted purities are 99.98% (O_2), 99.999% (Ar) and $\geq$ 99.8% (*n*-butanol).

The temperature profiles, which are important input parameters in the modeling calculations, are measured with laser-induced fluorescence (LIF) using the frequency-doubled output of an optical parametric oscillator (Continuum Sunlite EX OPO) near 306 nm to excite the OH *A*–*X* (0,0) transition. We estimate the accuracy of the temperature measurements to be ±150 K in the postflame and reaction zones and somewhat larger in the preheat zone, where the OH concentration is much smaller and its concentration gradient much steeper. We assume the temperature of the burner surface to be 500 K. The effect of temperature uncertainties on modeling computations has been illustrated in ref. 37, where it was shown that even worst-case disturbances to the measured temperature profile do not alter mechanistic conclusions provided by the kinetic model, but are responsible for disparities in species location between measurement and modeling results. The measured profiles are subsequently smoothed and used as input for the model calculations. The temperature profiles used in this study are available as supplemental material.†

The isomer-resolved chemical structures of the premixed *n*-butanol Flames 1–3, which are used as targets to test the model's performance, are determined by flame-sampling molecular-beam mass spectrometry (MBMS). The experiments are carried out at the Advanced Light Source (ALS) of the Lawrence Berkeley National Laboratory using photoionization by tunable synchrotron-generated vacuum-ultraviolet (VUV) radiation. A detailed description of the technique, the custom-built mass spectrometer and the data analysis procedures have been published elsewhere.[38–41] The instrument consists of a low-pressure flame chamber, a differentially pumped molecular-beam flame-sampling system, and a linear time-of-flight mass spectrometer with a resolution of $m/\Delta m \sim 500$. It is coupled to a 3-m monochromotor used to disperse the synchrotron radiation, which is tunable over the energy range from 8 to 17 eV with an energy resolution of 40 meV (fwhm). The burner is mounted on a translational stage which allows movements with high precision towards the respective sampling position within the flame. It is estimated that for the measurements presented here, the spatial location has an absolute accuracy of approximately ±0.5 mm. In this paper "Distance from Burner" refers to the actual separation between the tip of the sampling cone and the burner face, with no correction for probe sampling effects.

Species are identified both by mass-to-charge (m/z) ratios and by ionization thresholds from photon-energy scans at fixed burner locations.[39,41] An example is shown in Fig. 1 in which the flame-sampled (Flame 3) photoionization efficiency (PIE) curve of $m/z = 56$ (C_4H_8 and C_3H_4O) is shown together with PIE curves of 1-butene,[42] 2-butene,[42] and acrolein.[43] As can be seen, the flame-sampled PIE curve matches the PIE curve of 2-butene from its ionization energy (IE) at 9.10 eV up to a photon energy of about 9.55 eV, the IE of 1-butene. Contributions from acrolein appear at photon energies above its IE of 10.11 eV. Furthermore, *n*-butanol undergoes dissociative ionization, resulting in contributions at $m/z = 56$ above an appearance energy (AE) of 10.18 eV.[44] This example shows that determining the chemical composition at each mass peak

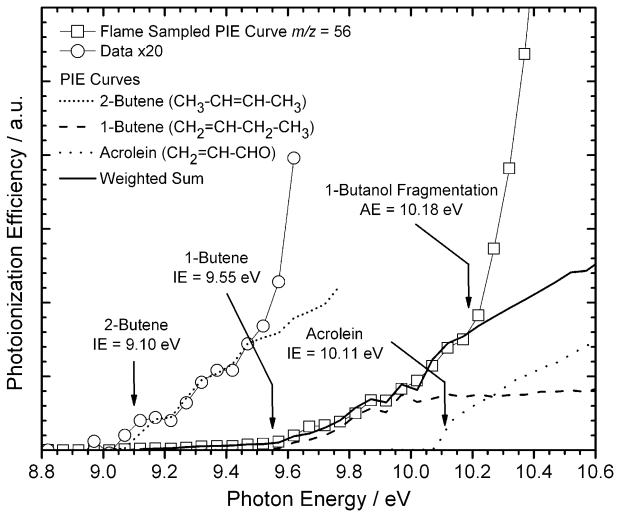

Fig. 1 Comparison of the flame-sampled PIE curve (connected symbols) at $m/z = 56$ from Flame 3 with PIE curves of 2-butene (short dots, ref. 42), 1-butene (dash, ref. 42), and acrolein (dots, ref. 43). The weighted sum, which includes contributions from 2-butene, 1-butene, and acrolein, is shown as solid line. Furthermore, contributions from dissociative ionization of *n*-butanol are visible above the appearance energy (AE) of 10.18 eV.

is a prerequisite for a quantitative analysis of the raw mass spectra. To derive accurate mole fraction profiles, it is also essential to understand the interferences caused by dissociative ionization of species of higher masses than that of the targeted species.

Ion signals are then measured as a function of distance from the burner and analyzed in order to produce quantitative mole fraction profiles for comparison with the modeling results. Photoionization cross sections needed in the flame-data analysis, including fragmentation patterns, are taken from ref. 42, 45–48, measured according to the procedures described in ref. 42, or estimated from those of similar molecules. For the intermediates with estimated photoionization cross sections the error of the reported mole fraction can be as large as a factor of four. In total, mole fraction profiles as a function of distance from the burner are measured for more than 40 flame species ranging from $m/z = 2$ (H_2) to $m/z = 74$ (*n*-butanol). These isomer-resolved species profiles provide a new opportunity to test and improve the detailed chemical mechanism for the high-temperature oxidation chemistry of *n*-butanol. But only the critical aspects of the chemical compositions of the flames are discussed here. The complete dataset is available as supplemental material.†

4. Flame chemistry insights

4.1. *n*-Butanol oxidation

It is well known that flames are highly reactive systems in which a vast number of fuel decomposition reactions can occur, including H-atom abstraction by mainly H, O, and OH and simple or complex bond fissions.[49] In *n*-butanol there are a total of 10 different H-abstraction sites, however H-abstraction reactions from the same C-atom are treated equally. In the commonly used nomenclature, the carbon atoms are distinguished as α-, β-, γ-, or δ-C with the α-C attached to the OH group.

Hydrogen abstraction reactions from the α-position in *n*-butanol are preferred because the corresponding C–H bond is weaker by ~16–27 kJ/mol compared with the other C–H bonds and by ~42 kJ/mol compared with the O–H bond.[20] RMG-estimated or calculated rate coefficients are taken from ref. 14 for the following important H-atom abstraction reactions:

$$CH_3CH_2CH_2CH_2OH + X \rightleftarrows CH_2CH_2CH_2CH_2OH\ (\delta\text{-}C_4H_9O) + HX \quad (R1a)$$

$$CH_3CH_2CH_2CH_2OH + X \rightleftarrows CH_3CHCH_2CH_2OH\ (\gamma\text{-}C_4H_9O) + HX \quad (R1b)$$

$$CH_3CH_2CH_2CH_2OH + X \rightleftarrows CH_3CH_2CHCH_2OH\ (\beta\text{-}C_4H_9O) + HX \quad (R1c)$$

$$CH_3CH_2CH_2CH_2OH + X \rightleftarrows CH_3CH_2CH_2CHOH\ (\alpha\text{-}C_4H_9O) + HX \quad (R1d)$$

$$CH_3CH_2CH_2CH_2OH + X \rightleftarrows CH_3CH_2CH_2CH_2O\ (\omega\text{-}C_4H_9O) + HX \quad (R1e)$$

with X = H, O, OH, O_2, HO_2, and CH_3. The unimolecular decomposition of *n*-butanol through simple and complex bond fission is also included in the model's predictions as described in ref. 14. The weakest bond in the molecule is the Cα–Cβ bond, but fission of the other C–C bonds cannot be ruled out, while the breaking of the C–O bond is not likely to be competitive

$$CH_3CH_2CH_2CH_2OH \rightleftarrows CH_3 + CH_2CH_2CH_2OH \quad (R2a)$$

$$\rightleftarrows CH_3CH_2 + CH_2CH_2OH \quad (R2b)$$

$$\rightleftarrows CH_3CH_2CH_2 + CH_2OH \quad (R2c)$$

The high-*p*-limit kinetics for the radical recombinations is set to 1×10^{13} cm^3 mol^{-1} s^{-1}. Complex bond fission is considered in this model as a four-centered elimination of water, forming 1-butene:

$$CH_3CH_2CH_2CH_2OH \rightleftarrows CH_3CH_2CHCH_2 + H_2O \quad (R3)$$

The water elimination's kinetics was computed using transition state theory and CBS-QB3, treating the low-frequency torsional modes as 1-d separable hindered rotors.[14] The computed rate coefficient is $1.59 \times 10^3 (T/1\ \mathrm{K})^{2.80} \exp(-62.0\ \mathrm{kcal/mol/RT}) \mathrm{s}^{-1}$. All these fuel-consumption reactions are represented schematically in Fig. 2.

The model predicts the overall fuel-consumption and product formation quite accurately, as shown by the agreement between experimental and modeled mole fractions of the major species (H_2, H_2O, CO, O_2, Ar, CO_2, and *n*-butanol). These profiles are shown in Fig. 3 as a function of distance from the burner for all four flames studied here. As can be seen from this comparison, the measured exhaust gas compositions at 30 mm away from the burner surface reach thermodynamic equilibrium values for the given temperature. The expected increase in the CO-to-CO_2 ratio as the stoichiometry ϕ is increased is also observed.

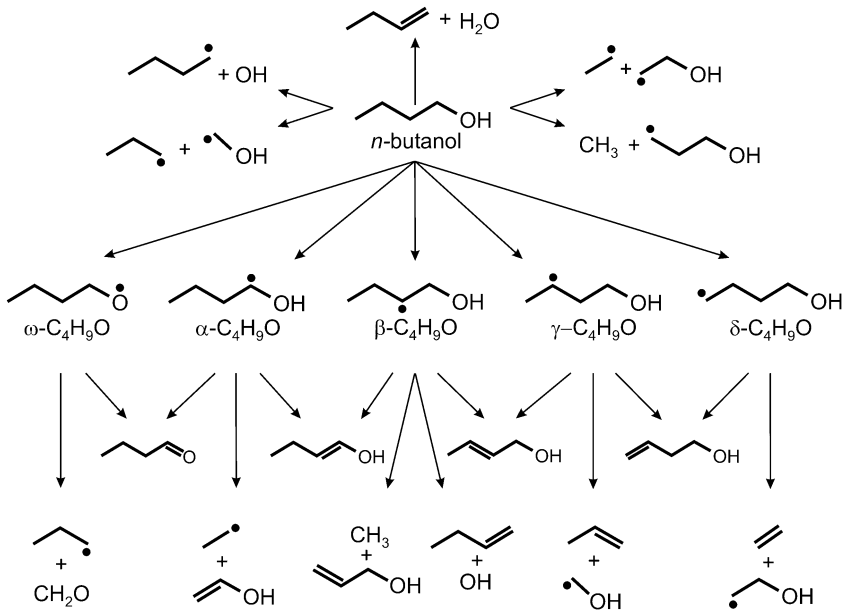

Fig. 2 Primary and secondary fuel-consumption pathways for *n*-butanol in low-pressure premixed flames.

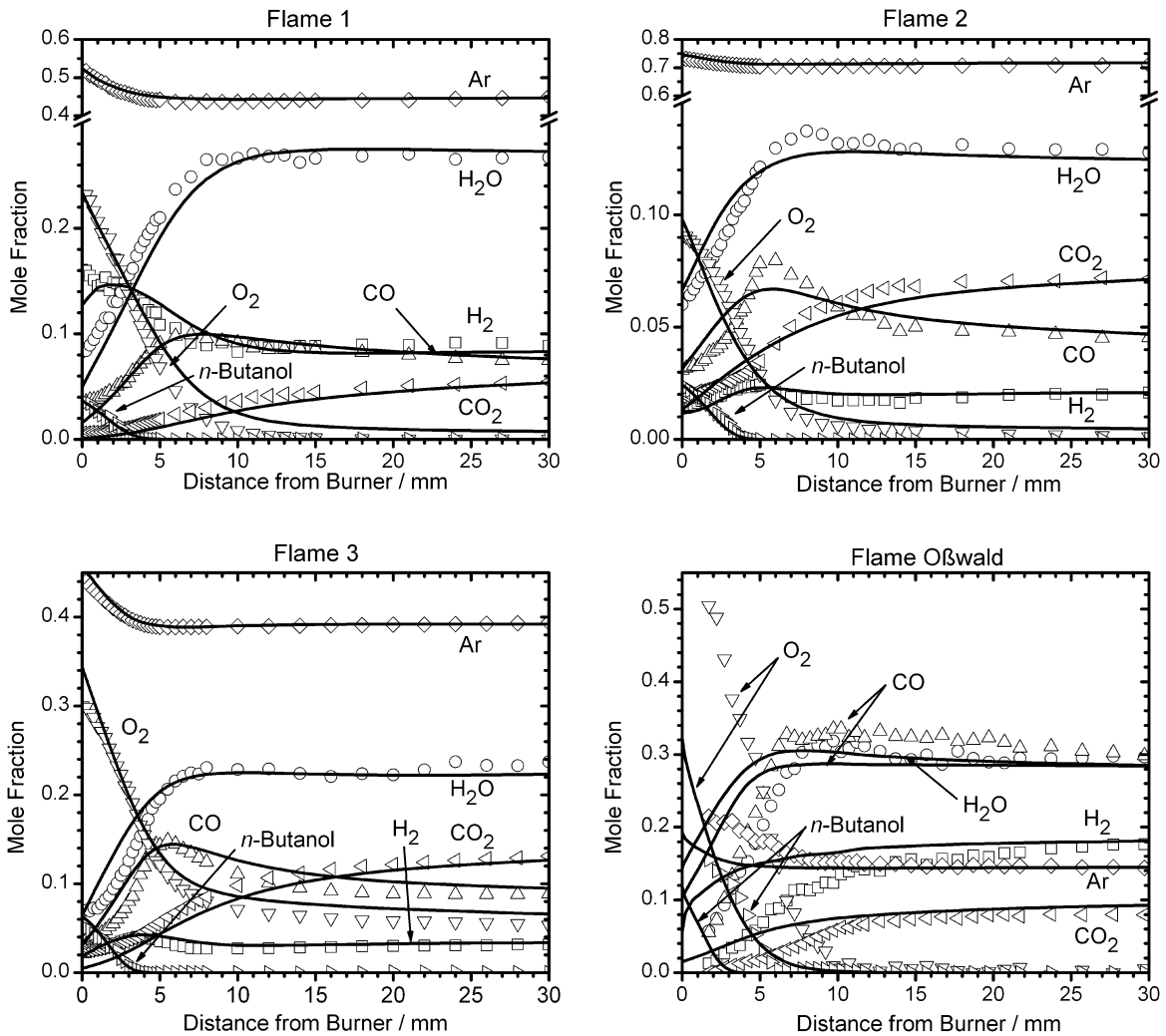

Fig. 3 Experimental (symbols) and modeled (lines) mole fraction profiles for the major species H_2, H_2O, CO, O_2, Ar, CO_2, and *n*-butanol as a function of distance from the burner for all four flames studied here. The experimental data for "Flame Oßwald" are from ref. 11.

As mentioned above, the experimental temperature profile and the mole fraction profiles are not shifted to account for possible probe effects.[50] Overall, we estimate the accuracy of the experimental major species profiles to be within 20%. Therefore, the agreement between experiment and model is mostly within the stated accuracy. For Flames 1–3 only small discrepancies are apparent very near the burner surface, where uncertainties in local temperature and flame-/sampling-probe interactions can be expected. However, the current model provides poor results close to the burner surface for the flame reported by Oßwald *et al.*[11] The temperature near the burner surface appears to be too high in the model, and thus the fuel is being consumed too rapidly. Therefore, modeling results for this flame should be interpreted with caution.

As just discussed, the model predicts the *n*-butanol mole fraction profile, *i.e.* the *n*-butanol consumption, very well for the conditions of this study, thus allowing for an assessment of the importance of various fuel-consumption pathways. Consequently, a reaction path analysis is performed, in order to identify the main pathways of fuel consumption and product formation. The characteristic consumption paths for *n*-butanol as predicted by the model are illustrated in Fig. 4. The model's predictions suggest that for all three flames the *n*-butanol chemistry occurs in the range 0–6 mm from the burner surface. The main decomposition routes are predicted to be H-abstraction from *n*-butanol by H, O, and OH giving the different C_4H_9O radicals. In particular, the *n*-$C_4H_{10}O$ + OH ⇄ α-C_4H_9O + H_2O reaction seems to be prominent in all flames.

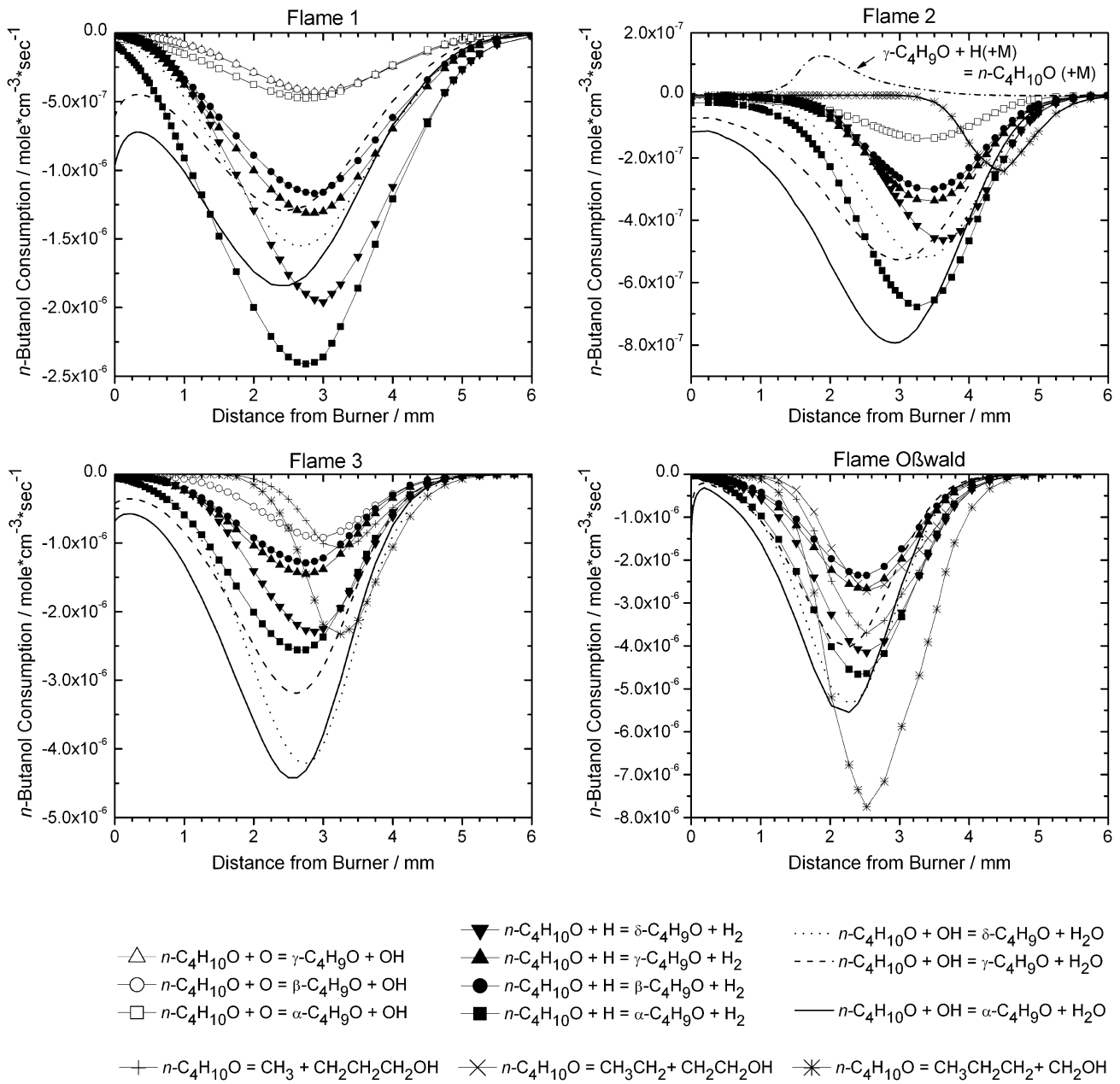

Fig. 4 The ten largest rates of *n*-butanol consumption in the four flames of this study, as predicted by the model.

In Flame (1), the rich *n*-butanol/H_2/O_2 base flame, abstraction of *n*-butanol by H atom and by OH radical contribute equally to the fuel's decomposition, whereas in Flames (2) and (3), abstraction by OH radical is the most dominant decomposition pathway. Within the group of the C_4H_9O radicals, the formation of the $CH_3CH_2CH_2CHOH$ (α-C_4H_9O) radical is predicted to be slightly preferred. The H-abstraction from the OH group (R1e) and the water-elimination reaction forming 1-butene (R3) are found to be not significant fuel-consumption pathways under any of the conditions described here. This result is in disagreement with the conclusions of Yang *et al.*,[6] who found the four-center elimination of water to produce 1-butene (R3) an important fuel consumption pathway under the low-pressure flame conditions of their study. This water-elimination channel (R3) was also found to be an important fuel consumption pathway for the non-premixed conditions of a study by McEnally and Pfefferle.[5] The fission of C–C bonds of *n*-butanol forming methyl and C_3H_6OH (R2a), ethyl and 2-hydroxyethyl (R2b), or *n*-propyl and hydroxymethyl (R2c) are only significant at high temperatures, as indicated in Flame (3) of this study and in the flame of Oßwald *et al.*[11] However, it is already discussed above that for the Oßwald *et al.* flame the comparison of the experimental and modeled mole fraction profiles of the major species may indicate that the temperature profile used in the model seems to be too hot close to the burner surface. The C–C bond fission reactions were also identified by Yang *et al.*[6] as major fuel consumption pathways.

4.2. C_4H_9O Radical decomposition and oxidation

For several reasons, the different C_4H_9O radical isomers cannot be distinguished experimentally. With the exception of the *n*-butoxy radical ($CH_3CH_2CH_2CH_2O$) the ionization energies of the C_4H_9O radicals are unknown. Furthermore, the signal intensity at m/z = 73 (C_4H_9O) is close to the detection limit of the experimental set-up, indicating that these radicals are consumed very fast. From the chemical point of view, these first-formed isomeric C_4H_9O radicals can isomerize, which has been found to be less important under the current conditions, or react with H and O_2 to form the butenol and *n*-butanal C_4H_8O isomers:

$$C_4H_9O + X\ (H \text{ or } O_2) \rightleftarrows C_4H_8O\ (n\text{-butanal or butenols}) + HX \quad (R4)$$

Furthermore, the C_4H_9O radicals can decompose by β-scission to form different oxygenated and non-oxygenated compounds.

$$\alpha\text{-}C_4H_9O \rightleftarrows CH_3CH_2CHCHOH + H \quad (R5a)$$

$$\rightleftarrows CH_3CH_2CH_2CHO + H \quad (R5b)$$

$$\rightleftarrows CH_3CH_2 + CH_2CHOH \quad (R5c)$$

Because C–C bonds are much weaker than C–H or O–H bonds, dissociation to ethyl and ethenol (R5c) is preferred. The possible formation of $CH_3CH_2CHCHOH$ (1-buten-1-ol) (R5a) is not favored energetically compared with the formation of the *n*-butanal (R5b). These reactions are included in Fig. 2, together with the similar reactions of the other C_4H_9O isomers:

$$\beta\text{-}C_4H_9O \rightleftarrows CH_3CH_2CHCHOH + H \quad (R6a)$$

$$\rightleftarrows CH_3CHCHCH_2OH + H \quad (R6b)$$

$$\rightleftarrows CH_3 + CH_2CHCH_2OH \quad (R6c)$$

$$\rightleftarrows CH_3CH_2CHCH_2 + OH \quad (R6d)$$

$$\gamma\text{-}C_4H_9O \rightleftarrows CH_2CHCH_2CH_2OH + H \quad (R7a)$$

$$\rightleftarrows CH_3CHCHCH_2OH + H \quad (R7b)$$

$$\rightleftarrows CH_3CHCH_2 + CH_2OH \quad (R7c)$$

$$\delta\text{-}C_4H_9O \rightleftarrows CH_2CHCH_2CH_2OH + H \quad (R8a)$$

$$\rightleftarrows CH_2CH_2 + CH_2CH_2OH \quad (R8b)$$

$$\omega\text{-}C_4H_9O \rightleftarrows CH_3CH_2CH_2 + CH_2O \quad (R9a)$$

$$\rightleftarrows CH_3CH_2CH_2CHO + H \quad (R9b)$$

For these reactions, the RMG-generated rate coefficient expressions are taken from ref. 14 and corrected for fall-off as described above. It is interesting to note that the decomposition of these radicals results in the formation of a number of different enols, including ethenol (R5c), 2-propen-1-ol (R6c), and the isomeric 1-buten-1-ol (R5a and R6a), 2-buten-1-ol (R6b and R7b), and 3-buten-1-ol (R7a and R8a). Reactions forming and removing these enolic species are therefore included in the reaction set together with thermochemistry and transport data. As shown in Fig. 2, other dissociation products include CH_3, C_2H_5, *n*-C_3H_7, CH_2OH, and CH_2CH_2OH radicals and CH_2O, C_3H_6 (propene), and C_4H_8 (1-butene).

The relative rates for formation and consumption of the α-, β-, γ-, and δ-C_4H_9O isomers are summarized graphically in Fig. 5. According to the modeling results of all four flames considered in this study, α-C_4H_9O is mainly consumed *via* reaction with O_2 forming either *n*-butanal (*n*-C_4H_8O; $CH_3CH_2CH_2CHO$) or 1-buten-1-ol (C_4H_8Oenol; $CH_3CH_2CHCHOH$):

$$\alpha\text{-}C_4H_9O + O_2 \rightleftarrows CH_3CH_2CH_2CHO + HO_2 \quad (R4a)$$

$$\alpha\text{-}C_4H_9O + O_2\ (+M) \rightleftarrows CH_3CH_2CHCHOH + HO_2\ (+M) \quad (R4b)$$

The rate coefficients for reaction (R4a) is estimated to be equal to the recent Zádor *et al.* estimate for $CH_3CHOH + O_2$.[32] Reaction (R4b) is the chemically-activated (well-skipping reaction) α-$C_4H_9O + O_2 \rightleftarrows CH_3CH_2CH_2CH(OO)OH \rightleftarrows CH_3CH_2CHCHOH + HO_2$, with the high-*p* kinetics for each reaction pathway being an RMG estimate (3.77×10^{12} cm^3 mol^{-1} s^{-1} and $6.6 \times 10^9 (T/1\ \text{K})^{1.01}$ exp(−29.6 kcal/mol/RT)s^{-1}, respectively); these high-*p* kinetics are within a factor of five of studies for the reactions $C_2H_5 + O_2 \rightleftarrows C_2H_5OO$ and $C_2H_5OO \rightleftarrows HO_2 + C_2H_4$.[51,52]

Minor contributions towards α-C_4H_9O consumption arise from β-scission to form C_2H_5 + ethenol (R5c) and H-addition/dissociation (chemically-activated) reactions forming C_3H_7 + CH_2OH, C_2H_5 + CH_2CH_2OH, or CH_3 + $CH_2CH_2CH_2OH$. These H-addition/dissociation reactions are also predicted to be important for the consumption of the β-, γ-, and δ-C_4H_9O radicals, as indicated in Fig. 5; to the authors' best knowledge, no other butanol mechanism in the literature includes these chemically-activated reactions, thus estimating the kinetics to

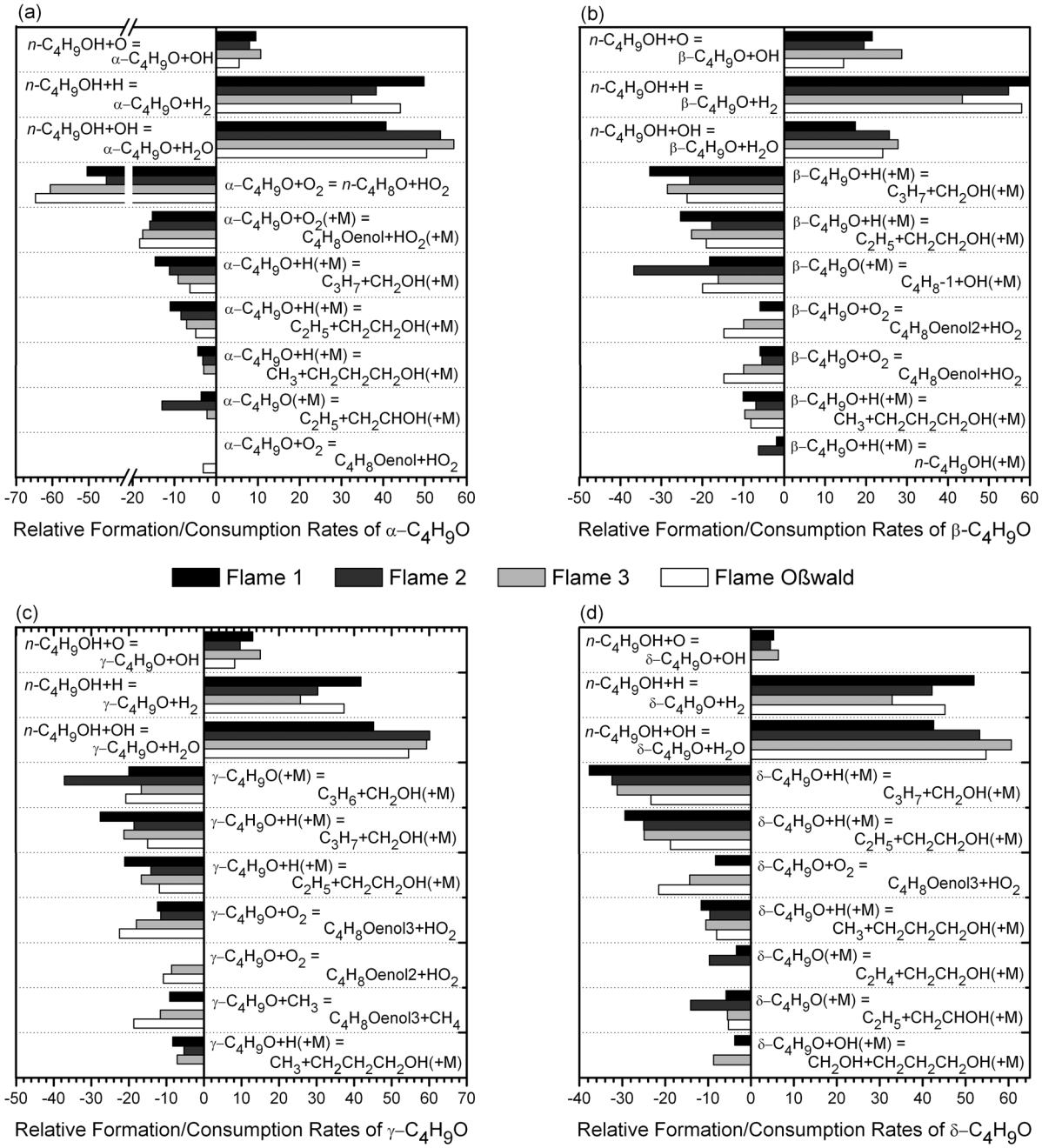

Fig. 5 Model predicted relative formation and consumption rates of the α-, β-, γ-, and δ-C_4H_9O radicals for the four flames of this study.

be effectively zero. However, one of the main consumption paths for β-C_4H_9O is a β-scission to 1-butene and OH:

$$\beta\text{-}C_4H_9O\ (+M) \rightleftarrows CH_2CHCH_2CH_3 + OH\ (+M) \quad (R10)$$

Other β-C_4H_9O removal steps, in addition to the previously-mentioned H-addition/dissociation reactions, include reactions with O_2 and OH to form 1-buten-1-ol (C_4H_8Oenol; $CH_3CH_2CHCHOH$) or 2-buten-1-ol (C_4H_8Oenol2; $CH_3CHCHCH_2OH$):

$$\beta\text{-}C_4H_9O + O_2 \rightleftarrows CH_3CHCHCH_2OH + HO_2 \quad (R4c)$$

$$\beta\text{-}C_4H_9O + O_2 \rightleftarrows CH_3CH_2CHCHOH + HO_2 \quad (R4d)$$

$$\beta\text{-}C_4H_9O + OH \rightleftarrows CH_3CHCHCH_2OH + H_2O \quad (R4e)$$

$$\beta\text{-}C_4H_9O + OH \rightleftarrows CH_3CH_2CHCHOH + H_2O \quad (R4f)$$

2-buten-1-ol is also formed as a product in the oxidation of γ-C_4H_9O radicals with O_2. However, this reaction represents only a minor channel and the formation of 3-buten-1-ol (C_4H_8Oenol3; $CH_2CHCH_2CH_2OH$) appears to be slightly more prominent; see Fig. 5(c):

$$\gamma\text{-}C_4H_9O + O_2 \rightleftarrows CH_2CHCH_2CH_2OH + HO_2 \quad (R4g)$$

The main γ-C_4H_9O consumption reaction is β-scission to form propene (C_3H_6) and CH_2OH:

$$\gamma\text{-}C_4H_9O\ (+M) \rightleftarrows C_3H_6 + CH_2OH\ (+M) \quad (R11)$$

However, the H-addition/dissociation reactions are also competitive in the consumption of the γ-C_4H_9O radical. For δ-C_4H_9O many different reactions contribute to its consumption, with the previously discussed H-addition/dissociation reactions being seemingly of greatest importance. Other reactions include oxidation by O_2 to form C_4H_8Oenol3

$$\delta\text{-}C_4H_9O + O_2 \rightleftarrows CH_2CHCH_2CH_2OH + HO_2 \quad (R4h)$$

and β-scission directly to form $C_2H_4 + CH_2CH_2OH$.

It is worth noticing that reaction (R4a) and (R10) are the respective main formation pathways for *n*-butanal and 1-butene. For the flames studied here, the experimental and modeled mole fraction profiles of these two species are shown in Fig. 6(a) and (b) for comparison. The fact that experimental and modeled *n*-butanal and 1-butene mole fraction profiles agree within the given error limits adds confidence to the model's predictive capabilities and to the description of the C_4H_9O formation and consumption. In the quantitative analysis of Oßwald *et al.*,[11] the individual contributions of *n*-butanal and 1-butene are not separated from their respective isomeric forms, butenols and 2-butene. Therefore, flame data from Oßwald *et al.*[11] are not included in Fig. 6.

4.3. Enol-aldehyde tautomerization

Since the work of Taatjes *et al.*,[53] steps have been undertaken to consider enol chemistry in combustion chemistry modeling. Black *et al.*[20] and Simmie and Curran[54] concluded, based on their studies, that enols play a "not insignificant" role[20] in the combustion of alcohols and that in these processes, enols should be almost as abundant as their isomeric carbonyl compounds.[54] A similar trend can be seen in the modeling results presented here. However, the current model overestimates the contributions of the butenol isomers when compared with the experimental results. Details are shown in Fig. 6(c), in which the model results are scaled down by a factor of five for easier comparison. This overprediction is not necessarily caused by too fast C_4H_9O consumption rates, but might also be caused by missing or slow butenol removal rates. The model includes unimolecular enol-aldehyde isomerization reactions and H-assisted reactions. For example, the C_2H_4O pressure-dependent network contains the following isomers and bimolecular product channels:

- Acetaldehyde (CH_3CHO)
- Ethenol (CH_2CHOH)
- $CH_2CHO + H$: formed by a C–H bond fission from acetaldehyde and by a O–H bond fission from ethenol
- $CH_3CO + H$: formed by a C–H bond fission from acetaldehyde
- $CH_3 + HCO$: formed by a C–C bond fission from acetaldehyde
- $CH_4 + CO$: formed by a unimolecular decomposition from acetaldehyde
- $CHCHOH + H$: formed by a C–H bond fission from ethenol
- $CH_2COH + H$: formed by a C–H bond fission from ethenol
- $CHCH_2 + OH$: formed by a C–O bond fission from ethenol
- The high-*p* kinetics for the direct unimolecular pathway from ethenol to acetaldehyde are from da Silva *et al.*:[55] $k(T) = 8.59 \times 10^{11}(T/1\ \mathrm{K})^{0.32} \exp(-55.9\ \mathrm{kcal/mol/RT})\mathrm{s}^{-1}$.

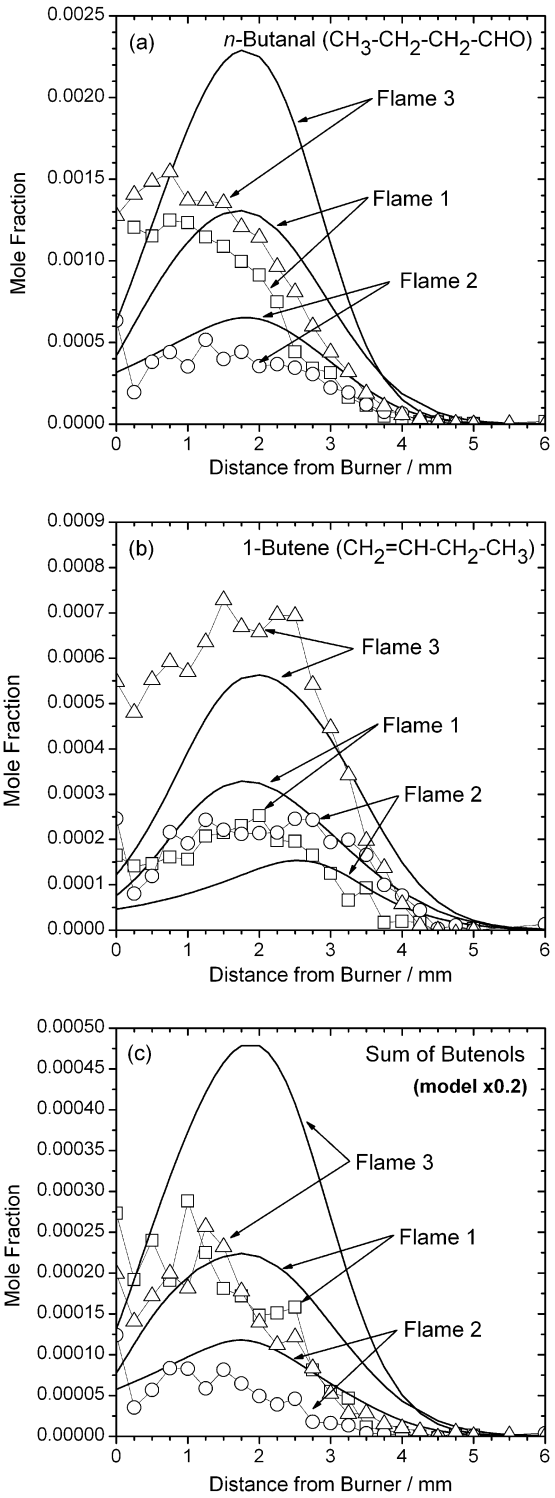

Fig. 6 Experimental mole fraction profiles (connected symbols) and modeled (lines) mole fractions in Flames 1–3 for (a) *n*-butanal, (b) 1-butene, and (c) the sum of the butenols. While for most species the model predictions are close to the experimental observations, there is a significant discrepancy for the butenols. The model results for the butenols have been scaled down by a factor of five for easy comparison.

The $k_\infty(T)$ for the other reactions in this network are estimated by the RMG software (using functional group analogies).

The thermochemistry for the species CH_2CHOH, CHCHOH, CH_2COH, and CH_3CO are estimated by RMG using Benson's group additivity and Bozzelli's hydrogen–atom bond increments, and these estimated thermodynamic properties are reported as supplemental material;† the remaining species thermochemistry comes from the GRI-Mech 3.0 mechanism. RMG estimates the 36 pressure-dependent rate coefficients using the methods described in Section 2.

For the H-assisted isomerization, the C_2H_5O pressure-dependent network contains:

- CH_2CH_2OH
- CH_3CHOH
- CH_3CH_2O
- CH_2CH_2 + OH: formed from a C–O β-scission from CH_2CH_2OH
- CH_2CHOH + H: formed from a C–H β-scission from CH_2CH_2OH and from a C–H β-scission from CH_3CHOH
- CH_3CHO + H: formed from a O–H β-scission from CH_3CHOH and from a C–H β-scission from CH_3CH_2O
- CH_3 + CH_2O: formed from a C–C β-scission from CH_3CH_2O
- CH_3CH_2 + O: formed from a C–O bond fission from CH_3CH_2O
- Isomerization reactions: $CH_2CH_2OH \rightleftarrows CH_3CHOH$, $CH_2CH_2OH \rightleftarrows CH_3CH_2O$, and $CH_3CHOH \rightleftarrows CH_3CH_2O$

All high-p rate coefficients are estimated by RMG. The thermochemistry for the species CH_2CH_2OH, CH_3CHOH, CH_3CH_2O, and CH_2CHOH are estimated by RMG using Benson's group additivity and Bozzelli's hydrogen–atom bond increments, and these estimated thermodynamic properties are also reported as supplementary material;† the remaining species thermochemistry comes from the GRI-Mech 3.0 mechanism. RMG estimates the 28 pressure-dependent rate coefficients using the methods described in Section 2.

Similar pressure-dependent networks exist for the propenols and butenols. Thus, although several enol decomposition pathways are present in the model, many of the parameters utilized in estimating the pressure-dependent kinetics are estimates themselves. Given that the model overestimates the butenol concentration, it appears that the current level of knowledge of the combustion chemistry of enols is still far from complete.

According to the modeling results, the decomposition of β-C_4H_9O to 2-propen-1-ol ($CH_2{=}CH{-}CH_2{-}OH$) and methyl radical is only a minor channel, as can be seen in Fig. 5(b). This finding is in agreement with the corresponding small experimentally observed mole fractions of propenols in all flames. However, propenol mole fractions are overpredicted by the current model by about a factor of five. According to the modeling results, the main pathways leading to propenol are through 1-buten-1-ol and 2-buten-1-ol *via* H-addition and methyl-radical elimination chemically-activated reactions. Therefore, an overprediction of the butenol isomers is leading to an overprediction of the propenol formed.

4.4. Small molecule chemistry

Besides those species which occur in the early fuel consumption processes, many more oxygenated and hydrocarbon intermediates are detected and predicted by the model. Most of these compounds are likely to result from further oxidation steps or molecular-growth reactions. In general, the model accurately predicts the mole fractions of many of these intermediates and products, including CH_3, C_2H_4, C_2H_5, CH_2CHOH, and C_3H_6. To exemplify these trends, a few selected experimental and modeled mole fraction profiles from within the four flames are shown in Fig. 7. Here, each species profile is shown only for one particular flame, however, it is worth pointing out that similar levels of agreement are observed for all flames. Profiles for the C_2 species acetylene, ethylene, and ethane are shown for Flame 1 in Fig. 7(a). The mole fraction profiles for oxygenated species (formaldehyde, acetaldehyde, and ethenol) are shown in 7(b) for Flame 2. To exemplify radical species predictions, mole fraction profiles of methyl, ethyl, and 1-methylallyl are shown in 7(c) for Flame 3. And finally, profiles for C_3 species (propargyl, propyne, and propene) are shown in 7(d) for the flame investigated by Oßwald *et al.*[11]

Overall, the model predicts the maximum mole fractions of most species within a factor of 2. Neither the experimental nor the modeled mole fraction profiles are shifted for better comparison. For CH_3 and C_2H_5, the predicted position of the maximum mole fraction is slightly further from the burner surface than the experimental values suggest. The source of the shift is not entirely obvious, but probe sampling effects and uncertainties in the temperature profiles are possible explanations. As pointed out earlier, the modeling results for the flame of Oßwald *et al.*[11] appears to be too close to the burner as evidenced in the mole fraction profiles of Fig. 3 and 7(d), in which the electron ionization data from ref. 11 are shown.

Although predicted ethenol and acetaldehyde mole fraction profiles agree within the expected uncertainties with the experimental results, we notice that ethenol is predicted to peak slightly above acetaldehyde levels. As discussed above, similar behavior of the model is observed for other enol/aldehyde isomeric pairs, including propenols/propanal and butenols/butanal, but this is not observed in the experiments. According to the model, the ethenol comes primarily from the direct dissociation of the α-C_4H_9O radical but also through other channels as speculated in ref. 56, *i.e.* C_2H_4 + OH reaction. Ethenol then reacts away to acetaldehyde, *via* both the unimolecular and H-atom assisted tautomerization reaction. The model underestimates the acetaldehyde profile for each of the three flames studied here. The dominant pathway to acetaldehyde is predicted to be the chemically-activated H-atom assisted tautomerization reaction, $CH_2CHOH + H(+M) \rightleftarrows CH_3CHO + H(+M)$, for all three flames; the direct tautomerization, corrected for fall-off effects, is predicted to be a minor route to acetaldehyde at higher temperatures. The H-abstraction of acetaldehyde by H atom, forming the acetyl radical, is predicted to be the dominant acetaldehyde decomposition pathway for all three flames. As mentioned in Section 4.3, several of the parameters used to solve the master equation for the C_2H_5O potential energy surface are estimates from RMG. Further work on obtaining more accurate estimates for these species thermochemistry and reaction rate coefficients would greatly aid in our modeling efforts, and in our understanding of these enol-aldehyde chemical species.

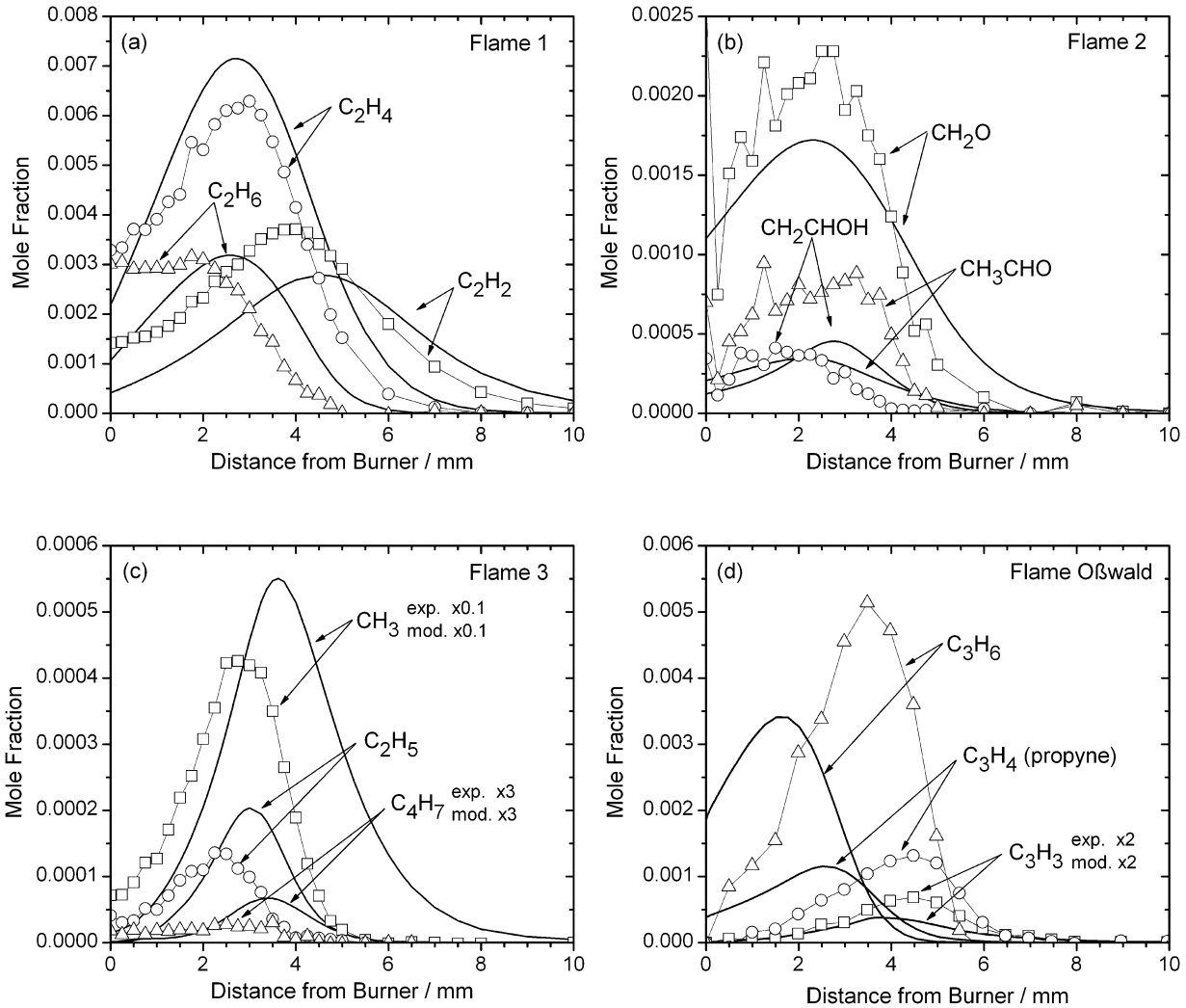

Fig. 7 Experimental mole fraction profiles (connected symbols) and modeled mole fractions (lines) for (a) C_2H_2, C_2H_4, and C_2H_6 in Flame 1, (b) CH_2O, CH_2CHOH, and CH_3CHO in Flame 2, (c) CH_3, C_2H_5, and C_4H_7 in Flame 3, and (d) C_3H_3, C_3H_4 (propyne), and C_3H_6 in the flame of Oßwald *et al.*[11] In (c) and (d), mole fraction profiles for CH_3, C_4H_7, and C_3H_3 are scaled for better visual comparison. Neither the experimental nor the modeled mole fraction profiles are shifted. There appears to be a discrepancy in the burner-face boundary conditions between the model and the experiments of Oßwald *et al.*[11]

5. Conclusions

This paper describes a detailed chemical mechanism for the combustion chemistry of *n*-butanol. A previously published version, which had been extensively tested against then available experimental data, is used here as a "Seed Mechanism", while the model is expanded to predict mole fraction profiles in burner-stabilized flames at low-pressures. The chemical structure of these flames is isomer-specifically resolved using flame-sampling molecular-beam mass spectrometry with tunable VUV synchrotron generation. This technique allows for a quantitative detection of enols, proving their significance in alcohol oxidation processes; however, the comparison with the model predictions reveals that the newly developed mechanism overpredicts their importance. It is speculated that this overprediction is not necessarily caused by too fast formation rates, but might also be caused by missing or slow consumption pathways. The model describes the initial *n*-butanol decomposition steps accurately, as evidenced in the very good agreement between experimental and modeled mole fraction profiles of *n*-butanol, *n*-butanal, and 1-butene. Under the conditions studied here, the latter species is almost exclusively formed by *β*-scission of the *β*-C_4H_9O radical ($CH_3CH_2^{\bullet}CHCH_2OH$); concerted-elimination of water is not an important *n*-butanol decomposition or 1-butene formation channel. The unimolecular dissociation of the fuel, *e.g.* C–C bond fission, is found to be only of minor importance. These reactions become competitive to the H-abstraction reactions with H, O, and OH, which normally dominate the fuel oxidation, only at the higher temperatures near the burner surface in the Flame (3) of the present study and in the flame studied by Oßwald *et al.* Subsequent disproportionation reactions of the C_4H_9O radicals, H-addition/dissociation reactions, and fast *β*-scissions govern the formation of smaller intermediates, with their profiles being predicted reasonably well.

The model for *n*-butanol combustion chemistry presented here, while not completely accurate, shows impressive fidelity to many distinct experimental data measured over a wide range

of conditions. In our future work we will apply this new model to predict the behavior of *n*-butanol in engines, where the sorts of detailed measurements reported here are not possible.

Acknowledgements

The work is supported by the US Department of Energy, Office of Basic Energy Sciences under the Energy Frontier Research Center for Combustion Science (Grant No. DE-SC0001198). The authors thank P. Oßwald, K. Kohse-Höinghaus, and F. Qi for sharing their unpublished (at the time) temperature and speciation data. The measurements are performed within the "Flame Team" collaboration at the Advanced Light Source (ALS), Lawrence Berkeley National Laboratory, Berkeley, USA, with Terrill Cool, Cornell University, as the principal investigator. The experiments have profited from the expert technical assistance of Paul Fugazzi. The Advanced Light Source is supported by the Director, Office of Science, Office of Basic Energy Sciences, of the U.S. Department of Energy under Contract No. DE-AC02-05CH11231. Sandia is a multi-program laboratory operated by Sandia Corporation, a Lockheed Martin Company, for the National Nuclear Security Administration under contract DE-AC04-94-AL85000.

References

1 P. Dürre, *Biotechnol. J.*, 2007, **2**, 1525–1534.
2 K. Kohse-Höinghaus, P. Oßwald, T. A. Cool, T. Kasper, N. Hansen, F. Qi, C. K. Westbrook and P. R. Westmoreland, *Angew. Chem., Int. Ed.*, 2010, **49**, 3572–3597.
3 P. S. Nigam and A. Singh, *Prog. Energy Combust. Sci.*, 2011, **37**, 52–68.
4 S. R. Smith, A. S. Gordon and M. H. Hunt, *J. Phys. Chem.*, 1957, **61**, 553–558.
5 C. S. McEnally and L. D. Pfefferle, *Proc. Combust. Inst.*, 2005, **30**, 1363–1370.
6 B. Yang, P. Oßwald, Y. Y. Li, J. Wang, L. X. Wei, Z. Y. Tian, F. Qi and K. Kohse-Höinghaus, *Combust. Flame*, 2007, **148**, 198–209.
7 S. M. Sarathy, M. J. Thomson, C. Togbe, P. Dagaut, F. Halter and C. Mounaim-Rousselle, *Combust. Flame*, 2009, **156**, 852–864.
8 X. L. Gu, Z. H. Huang, Q. Q. Li and C. L. Tang, *Energy Fuels*, 2009, **23**, 4900–4907.
9 P. S. Veloo, Y. L. Wang, F. N. Egolfopoulos and C. K. Westbrook, *Combust. Flame*, 2010, **157**, 1989–2004.
10 R. Grana, A. Frassoldati, T. Faravelli, U. Niemann, E. Ranzi, R. Seiser, R. Cattolica and K. Seshadri, *Combust. Flame*, 2010, **157**, 2137–2154.
11 P. Oßwald, H. Güldenberg, K. Kohse-Höinghaus, B. Yang, T. Yuan and F. Qi, *Combust. Flame*, 2011, **158**, 2–15.
12 J. A. Barnard, *Trans. Faraday Soc.*, 1957, **53**, 1423–1430.
13 K. M. Van Geem, S. P. Pyl, G. B. Marin, M. R. Harper and W. H. Green, *Ind. Eng. Chem. Res.*, 2010, **49**, 10399–10420.
14 M. R. Harper, K. M. Van Geem, S. P. Pyl, G. B. Marin and W. H. Green, *Combust. Flame*, 2011, **158**, 16–41.
15 P. Dagaut and C. Togbe, *Fuel*, 2008, **87**, 3313–3321.
16 P. Dagaut, S. M. Sarathy and M. J. Thomson, *Proc. Combust. Inst.*, 2009, **32**, 229–237.
17 P. Dagaut and C. Togbe, *Energy Fuels*, 2009, **23**, 3527–3535.
18 J. T. Moss, A. M. Berkowitz, M. A. Oehlschlaeger, J. Biet, V. Warth, P. A. Glaude and F. Battin-Leclerc, *J. Phys. Chem. A*, 2008, **112**, 10843–10855.
19 S. S. Vasu, D. F. Davidson, R. K. Hanson and D. M. Golden, *Chem. Phys. Lett.*, 2010, **497**, 26–29.
20 G. Black, H. J. Curran, S. Pichon, J. M. Simmie and V. Zhukov, *Combust. Flame*, 2010, **157**, 363–373.
21 K. A. Heufer, R. X. Fernandes, H. Olivier, J. Beeckmann, O. Röhl and N. Peters, *Proc. Combust. Inst.*, 2011, **33**, 359–366.
22 S. Vranckx, K. A. Heufer, C. Lee, H. Olivier, L. Schill, W. A. Kopp, K. Leonhard, C. A. Taatjes and R. X. Fernandes, *Combust. Flame*, 2011, **158**, 1444–1455.
23 B. W. Weber, K. Kumar, Y. Zhang and C.-J. Sung, *Combust. Flame*, 2011, **158**, 809–819.
24 C. K. Westbrook and F. L. Dryer, *Prog. Energy Combust. Sci.*, 1984, **10**, 1–57.
25 C. K. Law, *Proc. Combust. Inst.*, 2007, **31**, 1–29.
26 W. H. Green, J. W. Allen, R. W. Ashcraft, G. J. Beran, C. A. Class, C. Gao, C. F. Goldsmith, M. R. Harper, A. Jalan, G. R. Magoon, D. M. Matheu, S. M. Merchant, J. D. Mo, S. Petway, S. Raman, S. Sharma, J. Song, K. M. Van Geem, J. Wen, R. H. West, A. Wong, H.-W. Wong, P. E. Yelvington and J. Yu, *RMG - Reaction Mechanism Generator v3.3*, http://rmg.sourceforge.net, 2011.
27 R. G. Susnow, A. M. Dean, W. H. Green, P. Peczak and L. J. Broadbelt, *J. Phys. Chem. A*, 1997, **101**, 3731–3740.
28 N. J. B. Green and Z. A. Bhatti, *Phys. Chem. Chem. Phys.*, 2007, **9**, 4275–4290.
29 M. R. Harper, K. M. Van Geem, S. P. Pyl, S. M. Merchant, G. B. Marin and W. H. Green, *Combust. Flame*, 2011, **158**, 2075.
30 M. J. Frisch, G. W. Trucks, H. B. Schlegel, G. E. Scuseria, M. A. Rob, J. R. Cheeseman, J. A. M. Jr, T. Vreven, K. N. Kudin, J. C. Burant, J. M. Millam, S. S. Iyengar, J. Tomasi, V. Barone, B. Mennucci, M. Cossi, G. Scalmani, N. Rega, G. A. Petersson, H. Nakatsuji, M. Hada, M. Ehara, K. Toyota, R. Fukuda, J. Hasegawa, M. Ishida, T. Nakajima, Y. Honda, O. Kitao, H. Nakai, M. Klene, X. Li, J. E. Knox, H. P. Hratchian, J. B. Cross, V. Bakken, C. Adamo, J. Jaramillo, R. Gomperts, R. E. Stratmann, O. Yazyev, A. J. Austin, R. Cammi, C. Pomelli, J. W. Ochterski, P. Y. Ayala, K. Morokuma, G. A. Voth, P. Salvador, J. J. Dannenberg, V. G. Zakrzewski, S. Dapprich, A. D. Daniels, M. C. Strain, O. Farkas, D. K. Malick, A. D. Rabuck, K. Raghavachari, J. B. Foresman, J. V. Ortiz, Q. Cui, A. G. Baboul, S. Clifford, J. Cioslowski, B. B. Stefanov, G. Liu, A. Liashenko, P. Piskorz, I. Komaromi, R. L. Martin, D. J. Fox, T. Keith, M. A. Al-Laham, C. Y. Peng, A. Nanayakkara, M. Challacombe, P. M. W. Gill, B. Johnson, W. Chen, M. W. Wong, C. Gonzalez and J. A. Pople, *GAUSSIAN 03*, Gaussian, Inc., Wallingford, CT, 2003.
31 J. A. Miller, J. P. Senosiain, S. J. Klippenstein and Y. Georgievskii, *J. Phys. Chem. A*, 2008, **112**, 9429–9438.
32 J. Zádor, R. X. Fernandes, Y. Georgievskii, G. Meloni, C. A. Taatjes and J. A. Miller, *Proc. Combust. Inst.*, 2009, **32**, 271–277.
33 C. W. Zhou, J. M. Simmie and H. J. Curran, *Combust. Flame*, 2011, **158**, 726–731.
34 C. W. Wu, Y. P. Lee, S. C. Xu and M. C. Lin, *J. Phys. Chem. A*, 2007, **111**, 6693–6703.
35 N. Cohen and K. R. Westberg, *J. Phys. Chem. Ref. Data*, 1991, **20**, 1211–1311.
36 CHEMKIN-MFC, MFC 5.0, Reaction Design, San Diego, 2010.
37 S. Dooley, F. L. Dryer, B. Yang, J. Wang, T. A. Cool, T. Kasper and N. Hansen, *Combust. Flame*, 2011, **158**, 732–741.
38 T. A. Cool, K. Nakajima, C. A. Taatjes, A. McIlroy, P. R. Westmoreland, M. E. Law and A. Morel, *Proc. Combust. Inst.*, 2005, **30**, 1681–1688.
39 T. A. Cool, A. McIlroy, F. Qi, P. R. Westmoreland, L. Poisson, D. S. Peterka and M. Ahmed, *Rev. Sci. Instrum.*, 2005, **76**, 094102.
40 C. A. Taatjes, N. Hansen, D. L. Osborn, K. Kohse-Höinghaus, T. A. Cool and P. R. Westmoreland, *Phys. Chem. Chem. Phys.*, 2008, **10**, 20–34.
41 N. Hansen, T. A. Cool, P. R. Westmoreland and K. Kohse-Höinghaus, *Prog. Energy Combust. Sci.*, 2009, **35**, 168–191.
42 J. Wang, B. Yang, T. A. Cool, N. Hansen and T. Kasper, *Int. J. Mass Spectrom.*, 2008, **269**, 210–220.
43 C. A. Taatjes and O. Welz, personal communication.
44 J. D. Shao, T. Baer and D. K. Lewis, *J. Phys. Chem.*, 1988, **92**, 5123–5128.
45 J. C. Robinson, N. E. Sveum and D. M. Neumark, *J. Chem. Phys.*, 2003, **119**, 5311–5314.
46 J. C. Robinson, N. E. Sveum and D. M. Neumark, *Chem. Phys. Lett.*, 2004, **383**, 601–605.
47 T. A. Cool, J. Wang, K. Nakajima, C. A. Taatjes and A. McIlroy, *Int. J. Mass Spectrom.*, 2005, **269**, 210–220.

48 C. A. Taatjes, D. L. Osborn, T. M. Selby, G. Meloni, H. Y. Fan and S. T. Pratt, *J. Phys. Chem. A*, 2008, **112**, 9336–9343.
49 C. S. McEnally, L. D. Pfefferle, B. Atakan and K. Kohse-Höinghaus, *Prog. Energy Combust. Sci.*, 2006, **32**, 247–294.
50 U. Struckmeier, P. Oßwald, T. Kasper, L. Böhling, M. Heusing, M. Köhler, A. Brockhinke and K. Kohse-Höinghaus, *Z. Phys. Chem.*, 2009, **223**, 503–537.
51 R. Atkinson, D. L. Baulch, R. A. Cox, R. F. Hampson, J. A. Kerr, M. J. Rossi and J. Troe, *J. Phys. Chem. Ref. Data*, 1997, **26**, 521–1011.
52 J. A. Miller and S. J. Klippenstein, *Int. J. Chem. Kinet.*, 2001, **33**, 654–668.
53 C. A. Taatjes, N. Hansen, A. McIlroy, J. A. Miller, J. P. Senosiain, S. J. Klippenstein, F. Qi, L. S. Sheng, Y. W. Zhang, T. A. Cool, J. Wang, P. R. Westmoreland, M. E. Law, T. Kasper and K. Kohse-Höinghaus, *Science*, 2005, **308**, 1887–1889.
54 J. M. Simmie and H. J. Curran, *J. Phys. Chem. A*, 2009, **113**, 7834–7845.
55 G. da Silva, C. H. Kim and J. W. Bozzelli, *J. Phys. Chem. A*, 2006, **110**, 7925–7934.
56 C. A. Taatjes, N. Hansen, J. A. Miller, T. A. Cool, J. Wang, P. R. Westmoreland, M. E. Law, T. Kasper and K. Kohse-Höinghaus, *J. Phys. Chem. A*, 2006, **110**, 3254–3260.

